High-Resolution 3-D Imaging Algorithm With an Envelope of Modified Spheres for UWB Through-the-Wall Radars

Shouhei Kidera, *Associate Member, IEEE*, Takuya Sakamoto, *Member, IEEE*, and Toru Sato, *Member, IEEE*

***Abstract*—Through-the-wall imaging techniques with ultrawideband (UWB) radars are promising candidates for non-destructive testing and reliable human detection, especially in disaster areas, where victims are buried under collapsed walls. These applications require high-resolution target imaging to identify the object shape, such as a human body. We have already proposed a high-quality 3-dimensional (3-D) imaging algorithm in the form of Envelope, that is aimed at near field sensing for non-contact measurement or target identification for robots. Envelope achieves real-time accurate 3-D imaging with group mapping from multiple observed ranges to target points, and offers a reliable image even in noisy situations. However, this method does not maintain its quality for through-the-wall imaging because an observed range shift due to wall penetration causes a serious distortion in the image. This paper presents a high-resolution 3-D imaging algorithm by modifying the original Envelope, and which gives a more accurate object shape behind a wall. Furthermore, to enhance the resolution of the estimated images, this method is combined with a direct waveform compensation method, known as spectrum offset correction. Numerical simulations and an experiment verify that our proposed method achieves high-resolution 3-D imaging for through-the-wall radar applications.**

***Index Terms*—Direct waveform compensation, envelope of modified spheres, high-resolution 3-D imaging, through-the-wall radar, ultrawideband (UWB) pulse radar.**

I. Introduction

THROUGH-THE-WALL radar imaging has been investigated intensively for various applications, including non-destructive testing for precision devices, embedded in mortar, concrete or other electric materials. Reliable human detection in disaster areas, where survivors may be buried under collapsed walls or rubble, is one of the most useful applications thereof. It is also suitable for security systems in which radar is embedded in the walls so that the surveillance devices are invisible to intruders. These applications require fast high-resolution imaging to detect any object breakage or the small movements for a human body. While various through-the-wall radar algorithms have been proposed, one of these is applicable only to simple target shapes, such as points or spheres [1]–[3], and the others require intensive computation with data synthesis, such as synthetic aperture radar (SAR) [4], the time reversal method [5] or back scattering algorithms [6], [7]. The high-speed 3-D imaging algorithm, shape estimation algorithm based on BST and extraction of directly scattered waves (SEABED), which achieves real-time non-parametric 3-D imaging based on the reversible transforms boundary scattering transform (BST) and inverse BST (IBST) between the time delay and target boundary, has been proposed [8]–[10]. Although application examples of SEABED for through-the-wall imaging have been reported [11]–[13], these works cannot resolve the image distortions, completely, due to the range errors of wall penetrations, which depend on the thickness, and electric permittivity of the wall, or the incident angle to the wall. In the case of a thick wall, image accuracy decreases due to the range shift of the wall penetration. In addition, SEABED is quite sensitive to small range errors, because BST utilizes a derivative of the observed ranges.

On the contrary, the high-speed 3-D imaging algorithm, known as envelope, does not require derivative operations to create a stable image [14]–[16]. This method calculates spheres with observed delays for each antenna location and utilizes the principle that an arbitrary target boundary can be expressed as an outer or inner envelope of these spheres. The method enables us to achieve a robust imaging for arbitrary 3-D shapes with a group transforming ranges to target points. However, for through-the-wall imaging, Envelope has the same problem as SEABED, in that the observed range shift causes a non-negligible distortion in the image obtained.

As a solution to this problem, this paper describes a high-resolution and quick 3-D imaging algorithm that modifies the original Envelope method. The target surface is calculated as the envelope of modified spheres, that are deformed by the bent paths caused by the wall penetrations. The proposed algorithm offers an essential and strict solution to the problem occurring in the original Envelope, if electric permittivity and thickness of wall are known. The wall parameters can be estimated through other techniques. Wang, Zhou, and Kong [17] proposed an estimation algorithm for these parameters that assumes a point target. Wang and Amin [1] proposed another estimation algorithm based on minimizing the entropy of the estimated image.

In addition, this method can be combined with spectrum offset correction (SOC) [16], a range compensation method that

Manuscript received May 07, 2008; revised January 04, 2009. First published September 15, 2009; current version published November 04, 2009. This work was supported in part by the Grant-in-Aid for Scientific Research (A) under Grant 17206044 and in part by a Grant-in-Aid for JSPS Fellows under Grant 19-497.

S. Kidera is with the Department of Electronic Engineering, Graduate School of Electro-Communications, The University of Electro-Communications, Tokyo, Japan (e-mail: kidera@ee.uec.ac.jp).

T. Sakamoto and T. Sato are with the Department of Communications and Computer Engineering, Graduate School of Informatics, Kyoto University, Kyoto, Japan.

Digital Object Identifier 10.1109/TAP.2009.2032337

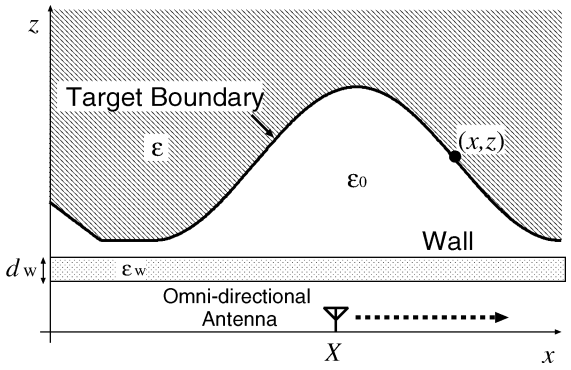

Fig. 1. System model in 2-D problem.

directly compensates the range shift due to scattered waveform deformation. First, we present the 2-D model of this method for simplicity. Then the method is extended to the 3-D model, and evaluated with numerical simulations and an experiment. In this evaluation, we investigate sensitivity to errors of wall parameters and the performance with various target shapes to clarify the applicability of the proposed method. The results verify that the proposed method achieves fast high-resolution 3-D imaging even for targets behind a thick wall.

II. 2-D Problem

A. System Model

Fig. 1 shows the system model for 2-D problem. It is assumed that the target has an arbitrary shape with a clear boundary, and that the propagation speed of the radio wave is a known constant. An omnidirectional antenna is scanned along the x-axis. A planar wall with a uniform relative permittivity $\epsilon_{\rm w}$ and thickness $d_{\rm w}$ is set parallel to the scanning axis. It is assumed that $\epsilon_{\rm w}$ and $d_{\rm w}$ are known constants. We utilize a ultrawideband (UWB) mono-cycle pulse as the transmitting current. R-space is defined as the real space in which the target and antenna are located, and is expressed by the parameter (x, z). These parameters are normalized by λ, which is the center wavelength of the pulse. We assume $z > 0$ for simplicity. $s(X, Z')$ is defined as the output of the matched filter to the received electric field at the antenna location $(x, z) = (X, 0)$, where $Z' = ct/(2\lambda)$ is expressed by the time t and the speed of the radio wave c. We connect the significant peaks of $s(X, Z')$ as Z for each X, and call this curve (X, Z) a quasi wavefront. D-space is defined as the space expressed by (X, Z). The transform from d-space to r-space corresponds to the imaging, dealt with in this paper.

B. Conventional Algorithms

1) SEABED: Previously, we proposed the high-speed imaging algorithm, known as SEABED, which utilizes a reversible transform BST between the point (x, z) in r-space and the point (X, Z) in d-space [8]. The inverse BST (IBST) is expressed as $x = X - Z\partial Z/\partial X, z = Z\sqrt{1-(\partial Z/\partial X)^2}$. This transform produces a strict solution if there is no other obstacle except the target. It has been reported that an application of SEABED for through-the-wall radar realizes high-speed target imaging behind a wooden wall [11], [12]. However, this work assumes quite a thin wall, and does not consider the range errors from passing through a medium with a different permittivity to that of air. The range compensation for this algorithm has been developed [13]; however, there is a serious image distortion because it fixes the amount of range shift for all incident angles. In addition, this algorithm suffers from instability caused by random noise because the IBST uses the derivative $\partial Z/\partial X$ that can enhance small fluctuations in a measured range. The fluctuation can be suppressed to some extent by a smoothing process. However, there is a trade-off between stability and resolution in a smoothing process [14]. Thus the stabilizing method degrades the resolution of the image obtained from the IBST. This cannot be prevented as long as the IBST is employed.

2) Envelope: To avoid the instability for small range errors, we previously proposed a stable high-speed imaging algorithm without derivative operations known as "envelope" [14]. This algorithm utilizes the principle that the target boundary can be expressed as an envelope of circles, with a center point $(X, 0)$ and radius Z. Envelope can estimate arbitrary shapes of targets because it does not use the derivative operation. However, it suffers from a large error in through-the-wall imaging because the observed range is shifted due to wall penetrations. This image distortion is non-negligible for target identification, such as a human body or precision devices.

C. Proposed Algorithm

To avoid the image distortions described in the previous section, we propose an accurate through-the-wall imaging algorithm by modifying the original Envelope. Each scattering path for wall penetration is strictly determined from Snell's law for each elevation angle. If the relative permittivity $\epsilon_{\rm w}$ and thickness of wall $d_{\rm w}$ are known constants, any range shift by the bent path can be solved. We utilize the extended principle of Envelope, that the target boundary (x, z) can be expressed as the envelope of the following curves:

$$\left.\begin{array}{rcl} x &=& X + \{Z + d_{\rm w}(1-\epsilon_{\rm w})\Psi(\phi)\}\cos\phi \\ z &=& d_{\rm w} + \{Z - \epsilon_{\rm w} d_{\rm w}\Psi(\phi)\}\sin\phi \end{array}\right\} \quad (1)$$

where the elevation angle ϕ is defined as $0 \le \phi \le \pi$, and

$$\Psi(\phi) = \frac{1}{\sqrt{\epsilon_{\rm w} - \cos^2\phi}} \quad (2)$$

is defined. Fig. 2 shows the relationship between the target boundary and the envelope of modified circles. This figure shows that the proposed method can be used not only for smooth shapes, but also arbitrary shapes including those with sharp edges. Here, we assume a convex target boundary for simplicity. This assumption simplifies the calculation of target boundary, that should be expressed as the outer envelope of the modified circles. The z coordinates of the convex target boundary for each given x is calculated as

$$z = \max_X [d_{\rm w} + \{Z - \epsilon_{\rm w} d_{\rm w}\Psi(\hat{\phi})\}\sin\hat{\phi}] \quad (3)$$

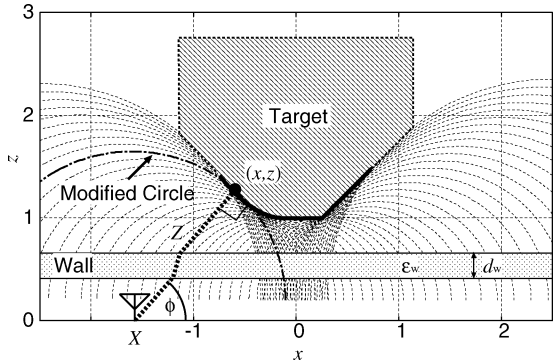

Fig. 2. Target boundary and envelope of modified circles.

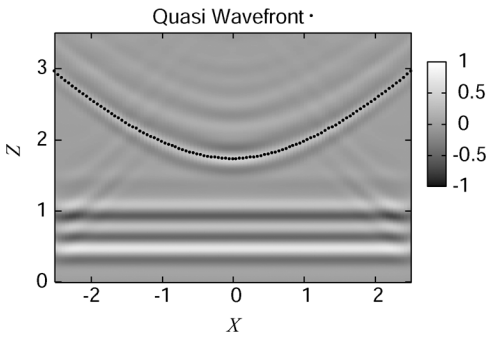

Fig. 3. Output of the matched filter and extracted quasi wavefront for each antenna location.

where $\hat{\phi}$ is determined by numerically solving the following equation about $\cos\hat{\phi}$, that is derived from the 1st term of (1) for a given x

$$Z^2\cos^4\hat{\phi} - 2Z(x-X)\cos^3\hat{\phi} + \left\{(x-X)^2 - Z^2\epsilon_{\rm w} + (\epsilon_{\rm w}-1)^2 d_{\rm w}^2\right\}\cos^2\hat{\phi} + 2(x-X)Z\epsilon_{\rm w}\cos\hat{\phi} - (x-X)^2\epsilon_{\rm w} = 0. \quad (4)$$

This algorithm can accurately estimate images where the actual parameters for the assumed wall, $d_{\rm w}$ and $\epsilon_{\rm w}$ are strictly known.

D. Performance Evaluation in Numerical Simulations

In this section, the performance of each algorithm is evaluated using numerical simulations. Here, a trapezoidal target is assumed and a planar wall is set for $0.5\lambda \le z \le 0.7\lambda$. The relative permittivity of the target is set to 1.0. The conductivity of the wall is 2.0×10^{-3} S/m, and $\epsilon_{\rm w} = 5.0$. The signals are received for $-2.5\lambda \le x, y \le 2.5\lambda$ at equal intervals of 0.1λ. The FDTD method is used for data generation. Fig. 3 shows the output of the matched filter and the extracted quasi wavefront for each antenna location. A noiseless situation is assumed. Fig. 4 shows the image estimated by SEABED with serious image distortion caused by range derivatives and range shifts due to the wall penetrations. Fig. 5 shows the image estimated by Envelope, using the same data as for SEABED. This proves that Envelope can produce a stable image since it does not use a derivative, that is the main difference between SEABED and Envelope. However, it suffers from a large error in the extracted boundary, and

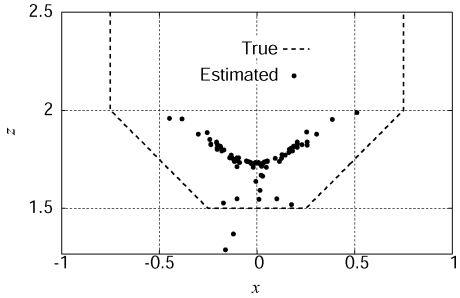

Fig. 4. Estimated image with SEABED.

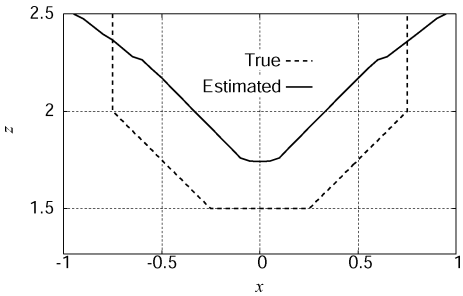

Fig. 5. Estimated image with Envelope.

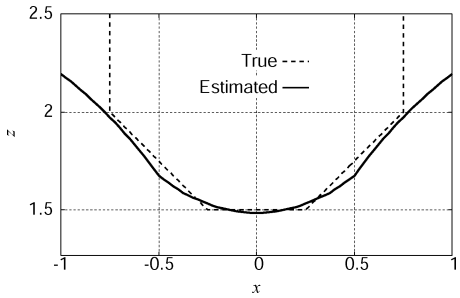

Fig. 6. Estimated image with the proposed method.

cannot reconstruct the correct target image. In this case, circles with large radii produce an incorrect envelope of circles.

On the contrary, Fig. 6 shows the estimated boundary after applying the proposed method to the same data as in Fig. 3. This figure shows that, by compensating the range shift of wall penetration, the image obtained is closer to the true target boundary than that obtained from the original Envelope. However, there are still small image distortions especially around the target edges. This is because the scattered waveform deformations cause the errors in observed ranges in the waveform matching. The waveform deformation is mainly caused by the frequency dependency of the size of the Fresnel zone [18], [19]. We have already developed a direct range compensation with spectrum offset correction for the deformed waveform, known as SOC [16]. SOC approximates the range shift ΔZ as

$$\Delta Z = (1 - f_{\rm tr}/f_{\rm sc})/W \quad (5)$$

$f_{\rm tr}$ and $f_{\rm sc}$ are the center frequencies of the transmitted and scattered waveform, respectively. $W = 4$ is constant, and is determined by the fractional bandwidth of the transmitted pulse. Fig. 7 shows the estimated image after the range compensations

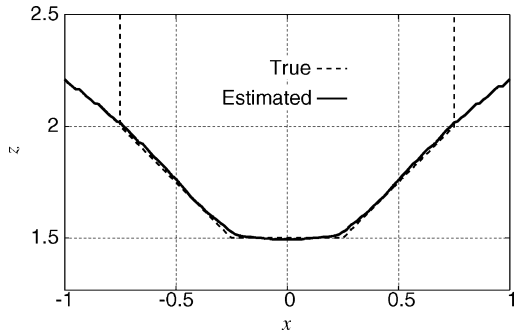

Fig. 7. Estimated image with the proposed method and SOC.

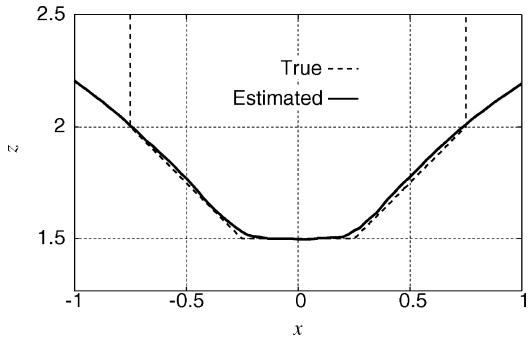

Fig. 8. Estimated image with the proposed method and SOC in $\mathrm{S/N} = 18$ dB.

by SOC. This verifies that the more accurate ranges Z improve the resolution around the edge region significantly, because the principle of this method offers a strict solution to the assumed inverse problem, if the correct quasi wavefront Z is obtained. The calculation time is around 0.2 sec for a Xeon 2.8 GHz processor. It is also confirmed that the scattered waveform holds its waveform, if the conductivity of wall is changed. Thus, the accuracy of the proposed method does not depend on the conductivity of the wall.

We also show an example of this method in a noisy situation, by adding white noises to the received signals. We assumed the same target boundary as in Fig. 4, and $\mathrm{S/N} = 18$ dB. Here, S/N is defined as the ratio of peak instantaneous signal power to the averaged noise power after applying the matched filter. Fig. 8 shows the estimated image for this noisy data, and this verifies that our algorithm accomplishes a stable high-resolution imaging. The reason for the stable imaging is that the algorithm does not utilize the derivative of the estimated ranges.

Furthermore, to ascertain the applicability of the proposed method in a realistic situation, sensitivity to errors in the wall parameters d_{w} and ϵ_{w} is evaluated. Here, the root mean square of the image error, e_{rms} is introduced as

$$e_{\mathrm{rms}} = \sqrt{\frac{\int_{x\in\gamma}\{z(x) - z_{\mathrm{true}}(x)\}^2 \mathrm{d}x}{\int_{x\in\gamma} \mathrm{d}x}} \tag{6}$$

where $z_{\mathrm{true}}(x)$ and $z(x)$ express the actual and estimated target boundaries, respectively. γ is the x range of the actual target. Fig. 9 shows e_{rms} for every d_{w} and ϵ_{w}, where the proposed method is applied to the same data as in Fig. 3. This result shows that each maximum error ratio for $e_{\mathrm{rms}} \leq 0.1\lambda$ is 25% for d_{w} and 18% for ϵ_{w}, respectively. Fig. 10 shows an example using the proposed method with the same data, where $d_{\mathrm{w}} = 0.16\lambda$ and $\epsilon_{\mathrm{w}} = 4.6$ are used for the calculation. In this case, $e_{\mathrm{rms}} = 0.09\lambda$ holds. The figure shows that the image has small offset errors on the z-axis, and that the proposed method produces a significant image that is not far from the actual one, even if the wall parameters have some errors.

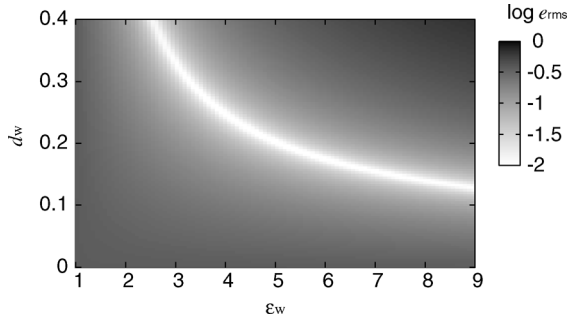

Fig. 9. e_{rms} for each wall parameter d_{w} and ϵ_{w}.

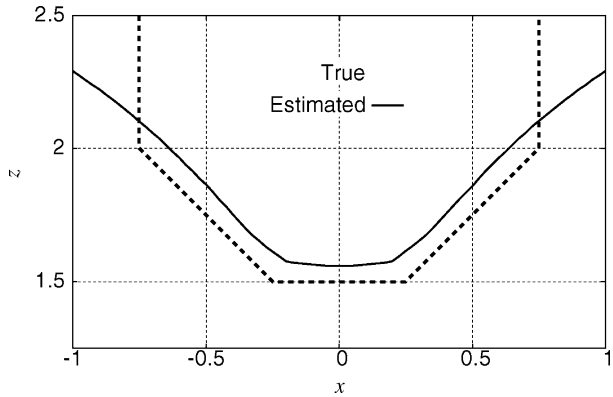

Fig. 10. Estimated image with the proposed method and SOC, where $d_{\mathrm{w}} = 0.16\lambda$ and $\epsilon_{\mathrm{w}} = 4.6$ are set.

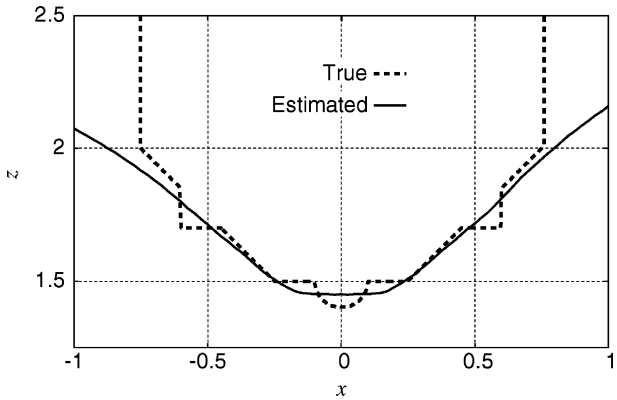

Fig. 11. Estimated image with the proposed method for the target with small extensions on its surface.

Finally, Fig. 11 shows an example for a target with small circle and triangle extensions on its boundary. This demonstration evaluates the case of a realistic target, such as an actual indoor target or a human body with small projections on its surface. Fig. 11 shows that the estimated image has a smooth surface and does not express the convex and concave edges correctly. This is because each antenna suffers from multiple in-

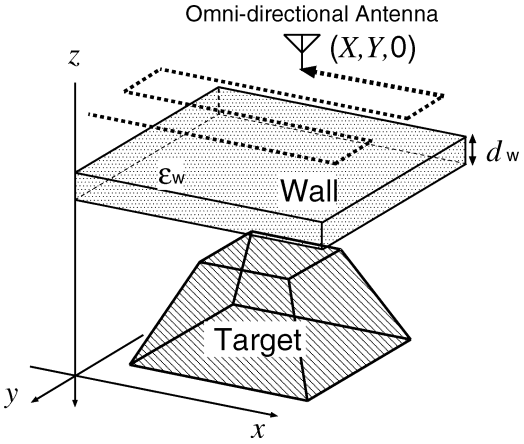

Fig. 12. System model in 3-D problem.

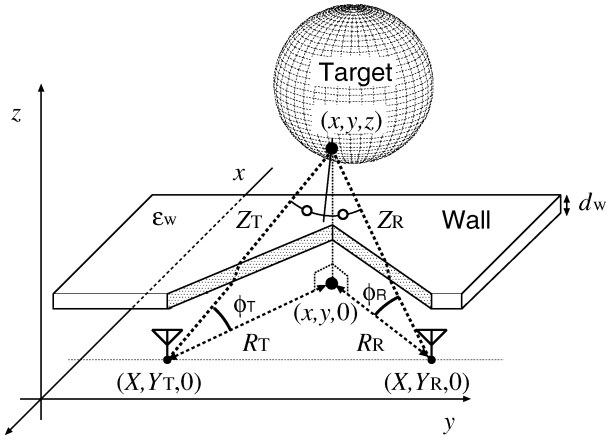

Fig. 13. Scattering path and target boundary in bi-static model.

terference echoes from the convex and concave boundaries, the variation length of which is less than wavelength. In general, this algorithm produces an accurate image where a target has smooth convex surfaces concatenated with discrete edges. Otherwise, a clear separation of the multiple echoes is difficult, and the proposed method suffers from small image distortions caused by the inaccuracy of the observed ranges, that cannot be compensated even with SOC. It is an important future work of ours to relax this target condition.

III. 3-D Problem

A. System Model

Fig. 12 shows the system model for a 3-D problem. The targets, antennas, and transmitted signals are the same as those described in the 2-D problem. An omnidirectional antenna is scanned on the plane, $z = 0$, and a linear polarization in the direction of the x-axis is assumed. A plane wall is set parallel to the $x-y$ plane, and $\epsilon_{\rm w}$ and $d_{\rm w}$ are known constants. R-space is the real space in which the target and antenna are located and is defined by the parameter (x, y, z). $s(X, Y, Z')$ is defined as the output of the matched filter to the received electric field at the antenna location $(x, y, z) = (X, Y, 0)$. We connect the significant peaks of $s(X, Y, Z')$ as Z for each X and Y, and call this surface (X, Y, Z) a quasi wavefront. D-space is defined as the space expressed by (X, Y, Z).

B. Conventional Algorithm

The original Envelope in 3-D model has been already proposed [16]. This algorithm is based on the principle that the target surface is expressed as an envelope of spheres with center $(X, Y, 0)$ and radius Z. This algorithm determines an arbitrary target boundary without derivative operations in free space. However, for through-the-wall imaging, the image obtained using Envelope is distorted due to the wall penetration for the same reasons as given in the 2-D problem.

C. Proposed Algorithm

To reconstruct a more accurate boundary, we extend the principle of Envelope for through-the-wall applications. Assuming a plane wall and Snell's law in the 3-D model leads to the fact that each scattering path exists on the same plane. Thus, a 3-D boundary extraction can readily be extended from that one in the 2-D problem. The proposed method expresses the target boundary as an envelope of the following surfaces:

$$\left.\begin{array}{rcl} x &=& X + \{Z + d_{\rm w}(1-\epsilon_{\rm w})\Psi(\phi)\}\cos\phi\cos\theta \\ y &=& Y + \{Z + d_{\rm w}(1-\epsilon_{\rm w})\Psi(\phi)\}\cos\phi\sin\theta \\ z &=& d_{\rm w} + \{Z - \epsilon_{\rm w} d_{\rm w}\Psi(\phi)\}\sin\phi \end{array}\right\} \quad (7)$$

where $0 \le \theta \le \pi$ and $0 \le \phi \le \pi/2$. This method is based on the principle that the convex target boundary behind a wall can be expressed as the outer envelope of these modified spheres. The z coordinates of the target boundary is calculated for each (x, y) as

$$z = \max_{X,Y}\{d_{\rm w} + \{Z - \epsilon_{\rm w} d_{\rm w}\Psi(\hat{\phi})\}\sin\hat{\phi}\} \quad (8)$$

where $\hat{\phi}$ can be solved from the 1st and 2nd equations in (7) for given (x, y). This algorithm gives a strict solution for a 3-D target surface extraction with edges or wedges behind a wall.

D. Extension to Bi-Static Model

This section describes extending the method to a bi-static model for the experimental investigation described in Section III.F, where the transmitter and receiver are mounted on the same platform. The location of the transmitting and receiving antennas are defined as $(X, Y_{\rm T}, 0)$ and $(X, Y_{\rm R}, 0)$, respectively. Fig. 13 shows the bent scattering path for bi-static radar scanning. $\phi_{\rm T}$ and $\phi_{\rm R}$ are defined as the elevation angle as shown in Fig. 13. Applying Snell's law to each scattering plane, the propagation distance $Z_{\rm T}$ and $Z_{\rm R}$ are expressed as

$$Z_{\rm T,R} = \frac{z - d_{\rm w}}{\sin\phi_{\rm T,R}} + \epsilon_{\rm w} d_{\rm w}\Psi(\phi_{\rm T,R}). \quad (9)$$

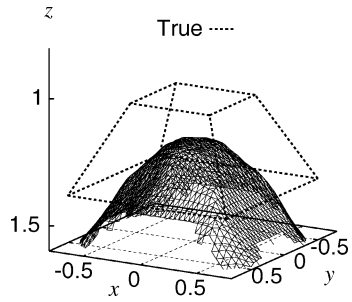

Fig. 14. Estimated image with Envelope in 3-D problem.

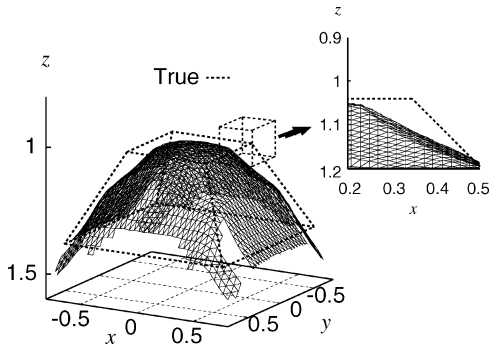

Fig. 15. Estimated image with the proposed method in 3-D problem.

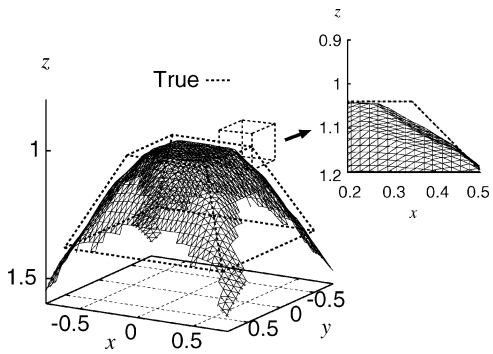

Fig. 16. Estimated image with the proposed method and SOC in 3-D problem.

Furthermore, the following equations hold

$$R_{\mathrm{T,R}} = \frac{z - d_{\mathrm{w}}}{\tan\phi_{\mathrm{T,R}}} + d_{\mathrm{w}}\Psi(\phi_{\mathrm{T,R}})\cos\phi_{\mathrm{T,R}} \tag{10}$$

where $R_{\mathrm{T}} = \sqrt{(X-x)^2 + (Y_{\mathrm{T}} - y)^2}$ and $R_{\mathrm{R}} = \sqrt{(X-x)^2 + (Y_{\mathrm{R}} - y)^2}$, for a given (x, y). Equations (9) and (10) derive the next relationship

$$\epsilon_{\mathrm{w}} R_{\mathrm{T}} \tan\phi_{\mathrm{T}} - Z_{\mathrm{T}} \sin\phi_{\mathrm{T}} = \epsilon_{\mathrm{w}} R_{\mathrm{R}} \tan\phi_{\mathrm{R}} - Z_{\mathrm{R}} \sin\phi_{\mathrm{R}}. \tag{11}$$

Equation (11) can be expanded to the 4th order equation for $\sin\phi_{\mathrm{R}}$ as

$$\begin{aligned} &Z_{\mathrm{R}}^2 \sin^4\phi_{\mathrm{R}} + 2Z_{\mathrm{R}}\alpha\sin^3\phi_{\mathrm{R}} \\ &+\left\{\alpha^2 - Z_{\mathrm{R}}^2 + \epsilon_{\mathrm{w}}^2 R_{\mathrm{R}}^2\right\}\sin^2\phi_{\mathrm{R}} - 2Z_{\mathrm{R}}\alpha\sin\phi_{\mathrm{R}} - \alpha^2 = 0 \end{aligned} \tag{12}$$

where $\alpha = \epsilon_{\mathrm{w}} R_{\mathrm{T}} \tan\phi_{\mathrm{T}} - Z_{\mathrm{T}} \sin\phi_{\mathrm{T}}$. If ϕ_{T} is given, (12) can be solved for ϕ_{R}. We define the solution to (12) as $\phi_{\mathrm{R}} = g(\phi_{\mathrm{T}})$. Then, z_{T} and z_{R} are derived from

$$z_{\mathrm{T}} = d_{\mathrm{w}} + \{Z_{\mathrm{T}} - \epsilon_{\mathrm{w}} d_{\mathrm{w}} \Psi(\phi_{\mathrm{T}})\}\sin\phi_{\mathrm{T}}, \tag{13}$$

$$z_{\mathrm{R}} = d_{\mathrm{w}} + \{2Z - Z_{\mathrm{T}} - \epsilon_{\mathrm{w}} d_{\mathrm{w}} \Psi(g(\phi_{\mathrm{T}}))\}\sin g(\phi_{\mathrm{T}}). \tag{14}$$

The possible elevation angle $\hat{\phi_{\mathrm{T}}}$ is calculated as

$$\hat{\phi_{\mathrm{T}}} = \arg\min_{\phi_{\mathrm{T}}} |z_{\mathrm{T}} - z_{\mathrm{R}}|. \tag{15}$$

The z-coordinate of each modified sphere for (X, Y, Z) is calculated as,

$$z_{(X,Y,Z)} = R_{\mathrm{T}} \tan\hat{\phi_{\mathrm{T}}} + d_{\mathrm{w}}\{1 - \Psi(\hat{\phi_{\mathrm{T}}})\sin\hat{\phi_{\mathrm{T}}}\}. \tag{16}$$

Finally, the z-coordinate of the convex target boundary is calculated for each given (x, y) as

$$z = \max_{X,Y} z_{(X,Y,Z)} \tag{17}$$

This algorithm also gives a strict surface extraction for a bi-static through-the-wall radar.

E. Performance Evaluation in Numerical Simulations

This section gives examples of applying the conventional and proposed methods to a through-the-wall 3-D imaging problem. Here, a mono-static radar is used. A trapezoidal target is assumed, and a plane wall is set parallel to the $x - y$ plane for $0.35\lambda \le z \le 0.49\lambda$. $\epsilon_{\mathrm{w}} = 5.0$ and $\sigma = 2.0 \times 10^{-3}$ S/m. We assume that ϵ_{w} and d_{w} are known constants. We receive signals for $-1.75\lambda \le x, y \le 1.75\lambda$ at equal intervals of 0.07λ. A noiseless situation is assumed. Fig. 14 shows the image produced by Envelope. It can be seen that the image has large errors along the z axis, and the estimated shape is significantly different from the actual one. Fig. 15 shows the image produced by the proposed method. This verifies that the proposed algorithm can produce a correct target 3-D image with accurately compensated ranges. Furthermore, Fig. 16 shows the estimated image using the proposed method after range compensation with SOC. This shows that the accuracy around the target edges is enhanced by compensating small range shift in the scattered waveform deformations.

To evaluate the characteristics of the estimated target surfaces, such as an edge or a smooth surface, the mean curvature H is introduced as

$$H = \frac{\left(1 + z_x^2\right) z_{yy} + \left(1 + z_y^2\right) z_{xx} - 2 z_x z_y z_{xy}}{2\left(1 + z_x^2 + z_y^2\right)^{3/2}} \tag{18}$$

where $z_x = (\partial z)/(\partial x)$ and, $z_{xy} = (\partial^2 z)/(\partial x \partial y)$. Here, a difference approximation is applied to the derivative calculation in order to avoid a singularity at an edge. H can specify the existence of edges or wedges, providing us significant information for recognizing a target shape. The left and right hands side of Fig. 17 show the mean curvatures for the estimated image using the proposed method and that with SOC, respectively. The region with large H in the proposed method with SOC expresses

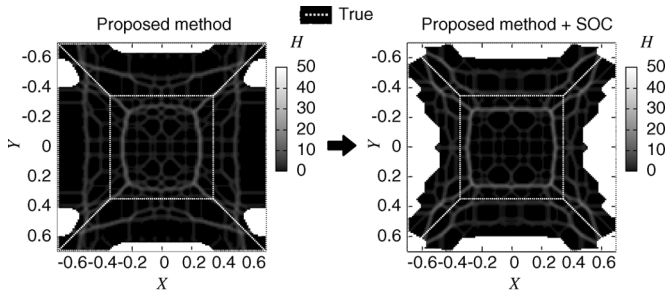

Fig. 17. Mean curvature H for the proposed method (left) and that with SOC (right).

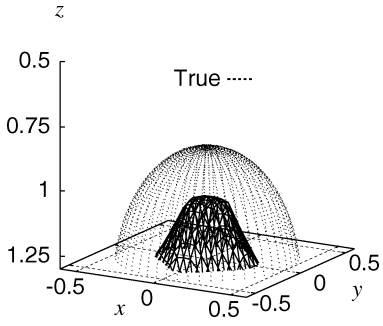

Fig. 18. Estimated image with Envelope for the sphere target.

an almost correct mean curvature around the edge or wedge regions of the actual shape. The calculation time for this imaging is about 4 s with a single Xeon 3.2 GHz processor. Furthermore, this example confirms that the proposed method can maintain its resolution and the stability of the image for $\mathrm{S/N} \geq 25$ dB.

Finally, examples of sphere and pyramid targets are presented to verify the flexibility of the proposed method. The wall parameters d_{w} and ϵ_{w} are the same as in the previous evaluation. Fig. 18 shows the image of a sphere target produced by Envelope. This image is severely distorted due to the range shift caused by wall penetration. The left and right hand sides of Fig. 19 show the obtained images produced by the proposed method and that by applying SOC, respectively. This figure verifies that the proposed method with SOC accurately expresses the smooth sphere surface. Figs. 20 and 21 show the same arrangement as in Fig. 18 and 19, respectively, for a pyramid shape target. These results show that the proposed method with SOC produces an accurate surface extraction, including the sharp edge and the wedge side on the pyramid. These evaluations confirm the applicability of the proposed method for various target identification or characteristic extractions.

F. Performance Evaluation in an Experiment

1) Experimental Setup: This section presents the experimental study of the proposed algorithm. We utilize a UWB pulse with a center frequency of 3.3 GHz and a 10 dB-bandwidth of 2.0 GHz. The bi-static radar system is used to avoid difficulties in the constitution of the mono-static system, where adequate isolation between the transmitted and received signals is difficult. The isolation between the two antennas is carried out by eliminating the direct wave, which can be measured in a case without a wall and target. The antenna with an elliptic

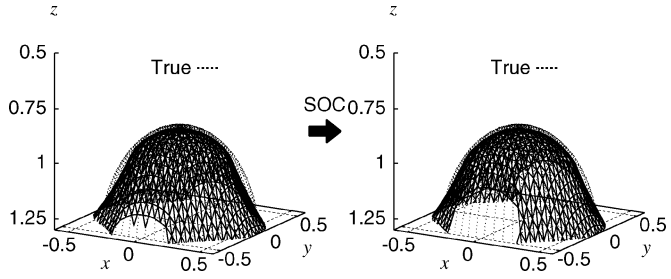

Fig. 19. Estimated image with the proposed method (left) and that with SOC (right) for the sphere target.

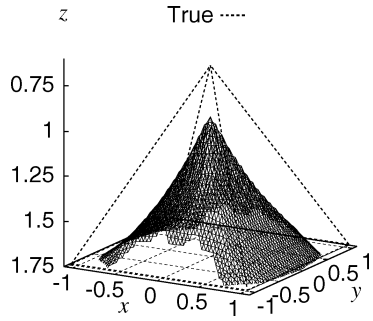

Fig. 20. Estimated image with Envelope for the pyramid target.

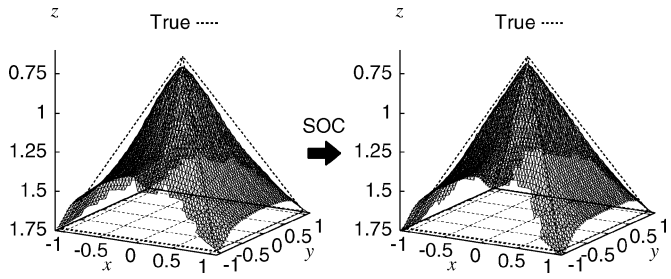

Fig. 21. Estimated image with the proposed method (left) and that with SOC (right) for the pyramid target.

polarization with the ratio of major to minor axis about 17 dB is used, since linear polarization is assumed in the numerical simulation. Any kind of polarization is, in principle, applicable to the proposed algorithm. The direction of the polarimetry axis of the antenna is along the y-axis. The 3 dB-beamwidth of the antenna is about 90°. The target has a trapezoidal shape, and constructed from stainless steel plates. We set a plane wall made of mortar, the thickness of which is 17 mm, and $\epsilon_{\mathrm{w}} = 4.79$, which is measured from the time delay of wall penetration. The conductivity of hydrated mortar is, in general, investigated from 0.02 to 0.05 S/m [20], in which the waveform deformation is negligible. Figs. 22 and 23 illustrates the arrangement of antennas with respect to the mortar plate and trapezoidal target, respectively. The wall is set parallel to the scanning plane. The transmitting and receiving antennas are scanned on the $z = 0$ plane, for $-200\ \mathrm{mm} \leq x \leq 200$ mm and $-150\ \mathrm{mm} \leq y \leq 200$ mm, respectively, with both sampling intervals set to 10 mm. The separation between the transmitting and receiving antennas is 75 mm in the y-direction. The data are coherently averaged 1024 times. The direct scattered signal from the trapezoidal target can be obtained by eliminating the

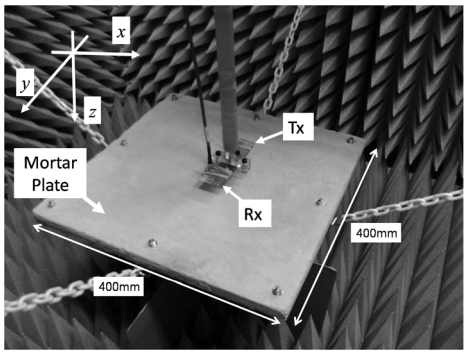

Fig. 22. Arrangement of antennas and mortar plate.

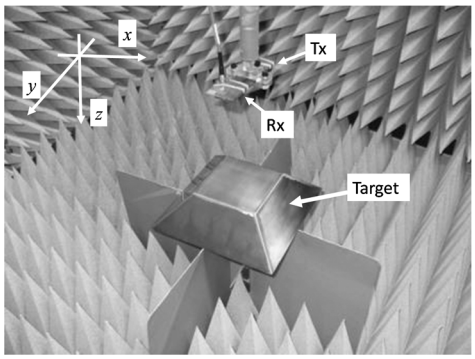

Fig. 23. Arrangement of antennas and trapezoidal target.

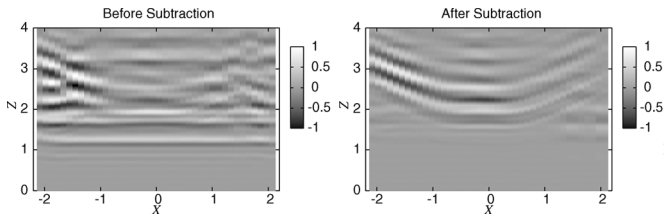

Fig. 24. Scattered signal before subtraction of wall reflection (left) and after subtraction of that (right) at $Y = 0.64$.

reflection signal from only the mortal plate without a target. In realistic situations, the elimination of the wall reflection wave is also possible by applying an appropriate time window to the received signal.

2) Performance of Experiment: The left and right sides of Fig. 24 shows the scattered waveform before and after subtraction of the wall reflections at $Y = 0.64$, respectively. Figs. 26 and 25 show the output of the matched filter for the scattered waveform at $Y = 0.64$ and $X = 0$, respectively. The amplitude of the received signals is not symmetrical for each of the X- and Y- axes due to the asymmetricity of the radiated antenna patterns. The S/N is around 24 dB. Fig. 27 shows the estimated image from the original Envelope using the experimental data. This figure shows that there is a non-negligible error for the z-axis due to wall penetration. Fig. 28 shows the image obtained from the proposed method after range compensation with SOC. Here, the bi-static extension of the proposed method described in Section III.D is used. This image has been reconstructed correctly, including the target edges. However, there are some image distortions around the region where $x \simeq 0.3$ or

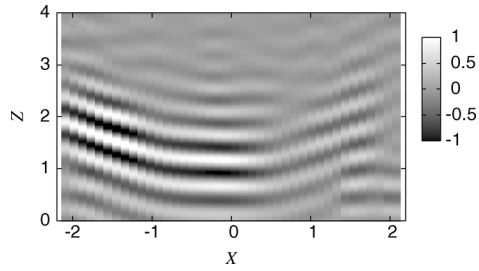

Fig. 25. Output of the matched filter at $Y = 0.64$ in the experiment.

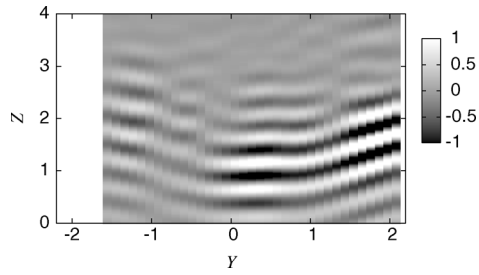

Fig. 26. Output of the matched filter at $X = 0$ in the experiment.

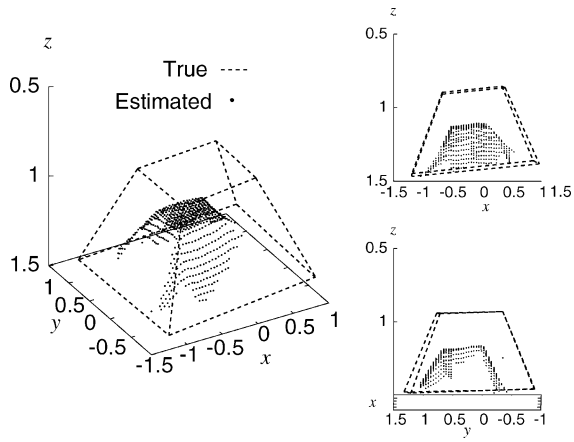

Fig. 27. Estimated image with Envelope in the experiment for the trapezoidal target.

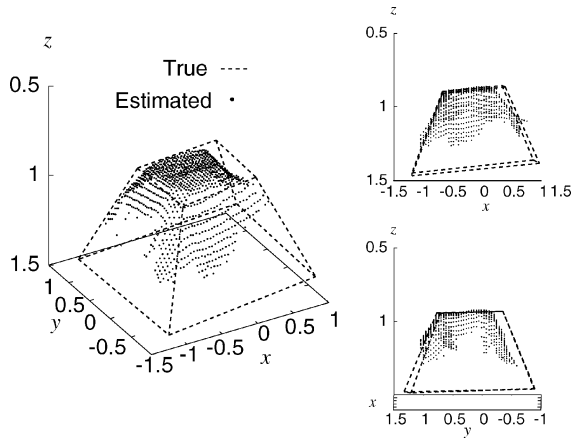

Fig. 28. Estimated image with the proposed method and SOC in the experiment for the trapezoidal target.

$y \simeq -0.5\lambda$ because the received signal from this region is quite small due to the asymmetricity of the antenna pattern as shown

in Figs. 26 and 25. In this region, the accuracy of the ranges deteriorates and this range error causes the distortions in the images. However, this distortion is not an substantial problem in the proposed method, and can be resolved by using antenna with a symmetric pattern.

IV. Conclusion

We have proposed a high-resolution high-speed imaging algorithm for through-the-wall radar by modifying the original Envelope. The target boundary behind the wall is expressed as an envelope of modified circles or spheres, which is determined from the electric permittivity and thickness of the wall. The numerical simulations confirmed that the proposed method accomplishes a fast higher-resolution imaging when compared to the conventional algorithms for 2-D and 3-D problems. In addition, image sensitivity to wall parameter errors and examples of various target shapes are demonstrated. These evaluations show the applicability of the proposed algorithm to realistic scenarios. Furthermore, we investigated the application examples in the experiment with a UWB signal by extending the bi-static model. These results show that our proposed algorithm maintains its high-quality imaging. We consider that this work contributes to the high-quality 3-D imaging required for human bodies buried under rubble or collapsed walls. Here, we should note that the image quality of the proposed method is often distorted in cases of more complex-shaped targets, because such kinds of targets create more complicated quasi wavefronts. As well, multiple scattered signals also cause false images. To overcome this difficulty, some extended algorithms have been developed for free space imaging. These improve the accuracy for complex-shaped targets without using a quasi wavefront [21], or enhance the visible range of target surfaces by making use of multiple scattered components for imaging [22]. Their extension to through-the-wall radar is an important issue for our future work.

References

[1] G. Wang and M. G. Amin, "Imaging through unknown walls using different standoff distances," *IEEE Trans. Signal Process.*, vol. 54, no. 10, pp. 4015–4025, Oct. 2006.

[2] F. Ahmad and M. G. Amin, "Noncoherent approach to through-the-wall radar localization," *IEEE Trans. Aerosp. Electron. Syst.*, vol. 42, no. 4, pp. 1405–1419, Oct. 2006.

[3] F. Ahmad, Y. Zhang, and M. G. Amin, "Three-dimensional wideband beamforming for imaging through a single wall," *IEEE Lett. Geosci. Remote Sens. Lett.*, vol. 5, no. 2, pp. 176–179, Apr. 2008.

[4] F. Ahmad, M. G. Amin, and S. A. Kassam, "Synthetic aperture beamformer for imaging through a dielectric wall," *IEEE Trans. Aerosp. Electron. Syst.*, vol. 41, no. 1, pp. 271–283, Jan. 2005.

[5] V. Chatelee, A. Dubois, M. Yedlin, I. Aliferis, J. Y. Dauvignac, and C. Pichot, "Time reversal of experimental ultra wideband microwave data in a through-the-wall (TTW) configuration," presented at the Electromagn. Theory Symp. (EMTS), Jul. 2007.

[6] J. Sachs, R. Herrmann, M. Kmec, M. Helbi, and K. Schilling, "Recent advances and applications of M-sequence based ultra-wideband sensors," presented at the Int. Conf. on UWB, Sep. 2007.

[7] R. Zetik, S. Crabbe, J. Krajnak, P. Peyerl, J. Sachs, and R. Thoma, "Detection and localization of person behind obstacles using M-sequence through-the-wall radar," in *Proc. SPIE*, 2006, vol. 6201.

[8] T. Sakamoto and T. Sato, "A target shape estimation algorithm for pulse radar systems based on boundary scattering transform," *IEICE Trans. Commun.*, vol. E87-B, no. 5, pp. 1357–1365, 2004.

[9] T. Sakamoto, "A fast algorithm for 3-dimensional imaging with UWB pulse radar systems," *IEICE Trans. Commun.*, vol. E90-B, no. 3, pp. 636–644, 2007.

[10] T. Sakamoto, S. Kidera, T. Sato, and S. Sugino, "An experimental study on a fast 3-D imaging algorithm for UWB pulse radars," *IEICE Trans. Commun.*, vol. J90-B, no. 1, pp. 66–73, 2007, (in Japanese).

[11] S. Hantscher, B. Praher, A. Reisezahn, and C. G. Diskus, "Analysis of imaging radar algorithms for the identification of targets by their surface shape," presented at the Int. Conf. on UWB, Sep. 2006.

[12] S. Hantscher, B. Etzlinger, A. Reisezahn, and C. G. Diskus, "A wave front extraction algorithm for high-resolution pulse based radar systems," presented at the Int. Conf. on UWB, Sep. 2007.

[13] S. Hantscher, A. Reisezahn, and C. G. Diskus, "Through-wall imaging with a 3-D UWB SAR algorithm," *IEEE Signal Process. Lett.*, vol. 15, pp. 269–272, 2008.

[14] S. Kidera, T. Sakamoto, and T. Sato, "A robust and fast imaging algorithm with an envelope of circles for UWB pulse radars," *IEICE Trans. Commun.*, vol. E90-B, no. 7, pp. 1801–1809, Jul. 2007.

[15] S. Kidera, T. Sakamoto, and T. Sato, "High-resolution and fast 3-D imaging algorithm with spectrum shift for UWB pulse radars," presented at the Eur. Conf. on Antenna and Propag., Nov. 2007, Th4.11.4.

[16] S. Kidera, T. Sakamoto, and T. Sato, "High-resolution and real-time UWB radar imaging algorithm with direct waveform compensations," *IEEE Trans. Geosci. Remote Sens.*, vol. 46, no. 11, pp. 3503–3513, 2008.

[17] H. Wang, Z. Zhou, and L. Kong, "Wall parameter estimation for moving target localization with through-the-wall radar," in *Proc. Int. Conf. on Microw. and Millimeter Wave Technol. ICMMT'07*, Apr. 2007, pp. 1–4.

[18] S. Kidera, T. Sakamoto, T. Sato, and S. Sugino, "An accurate imaging algorithm with scattered waveform estimation for UWB pulse radars," *IEICE Trans. Commun.*, vol. E89-B, no. 9, pp. 2588–2595, Sep. 2006.

[19] S. Kidera, T. Sakamoto, and T. Sato, "A high-resolution imaging algorithm without derivatives based on waveform estimation for UWB radars," *IEICE Trans. Commun.*, vol. E90-B, no. 6, pp. 1487–1494, Jun. 2007.

[20] J. D. Shane, T. O. Mason, and H. M. Jennings, "Effect of the interfacial transition zone on the conductivity of Portland cement mortars," *J. Amer. Ceramic Society*, vol. 83, no. 5, pp. 1137–1144, 2000.

[21] S. Kidera, T. Sakamoto, and T. Sato, "High-speed UWB radar imaging algorithm for complex target boundary without wavefront connection," presented at the XXIX General Assembly of URSI, Jul. 2008, BP17.2.

[22] S. Kidera, T. Sakamoto, and T. Sato, Shadow region imaging based on aperture synthesis of multiple scattering waves for UWB radars IEICE Tech. Rep., Jan. 2009, vol. 108, pp. PN2008–78, (in Japanese).

Shouhei Kidera (A'08) received the B.E. degree from Kyoto University, Kyoto, Japan, in 2003 and the M.I. and Ph.D. degrees from the Graduate School of Informatics, Kyoto University, in 2005 and 2007, respectively.

He is an Assistant Professor in the Department of Electronic Engineering, Graduate School of Electro-Communications, University of Electro-Communications, Japan. His current research interest is in advanced signal processing for the near field radar, UWB radar.

Dr. Kidera is a member of the Institute of Electronics, Information, and Communication Engineers of Japan (IEICE) and the Institute of Electrical Engineering of Japan (IEEJ).

Takuya Sakamoto (M'04) was born in Nara, Japan, in 1977. He received the B.E. degree from Kyoto University, Kyoto, Japan, in 2000 and the M.I. and Ph.D. degrees from the Graduate School of Informatics, Kyoto University, in 2002 and 2005, respectively.

He is an Assistant Professor in the Department of Communications and Computer Engineering, Graduate School of Informatics, Kyoto University. His current research interest is in signal processing for UWB pulse radars.

Dr. Sakamoto is a member of the Institute of Electronics, Information, and Communication Engineers of Japan (IEICE), and the Institute of Electrical Engineering of Japan (IEEJ).

Toru Sato (M'92) received the B.E., M.E., and Ph.D. degrees in electrical engineering from Kyoto University, Kyoto, Japan, in 1976, 1978, and 1982, respectively.

He has been with Kyoto University since 1983 and is currently a Professor in the Department of Communications and Computer Engineering, Graduate School of Informatics. His major research interests have been system design and signal processing aspects of atmospheric radars, radar remote sensing of the atmosphere, observations of precipitation using radar and satellite signals, radar observation of space debris, and imaging with UWB pulse radars.

Dr. Sato is a fellow of the Institute of Electronics, Information, and Communication Engineers of Japan, and a member of the Society of Geomagnetism and Earth, Planetary and Space Sciences, the Japan Society for Aeronautical and Space Sciences, the Institute of Electrical and Electronics Engineers, and the American Meteorological Society. He was awarded the Tanakadate Prize in 1986.